Thermodynamic and Kinetic Effects of N3′→P5′ Phosphoramidate Modification on Pyrimidine Motif Triplex DNA Formation†

Hidetaka Torigoe*

Tsukuba Life Science Center, The Institute of Physical and Chemical Research (RIKEN), 3-1-1 Koyadai, Tsukuba, Ibaraki 305-0074, Japan

Received August 11, 2000; Revised Manuscript Received November 13, 2000

ABSTRACT: I have investigated the thermodynamic and kinetic effects of N3′→P5′ phosphoramidate (PN) backbone modification of triplex-forming oligonucleotide (TFO) on the pyrimidine motif triplex formation between a 23-bp target duplex and a 15-mer TFO using electrophoretic mobility shift assay, UV melting, isothermal titration calorimetry, and interaction analysis system. The thermodynamic and kinetic analyses have clearly indicated that the PN modification of TFO not only significantly increased the thermal stability of the pyrimidine motif triplex at neutral pH but also increased the binding constant of the pyrimidine motif triplex formation at room temperature and neutral pH by nearly 2 orders of magnitude. The consideration of the observed thermodynamic parameters has suggested that the more rigidity of the PN TFO in the free state relative to the unmodified TFO may enable the significant increase in the binding constant of the pyrimidine motif triplex formation at neutral pH. Kinetic data have also demonstrated that the observed PN modification-mediated promotion of pyrimidine motif triplex formation at neutral pH resulted from the considerable decrease in the dissociation rate constant rather than the increase in the association rate constant. This information will present an effective approach for designing chemically modified TFO with higher binding affinity in the triplex formation under physiological conditions, which may eventually lead to progress in therapeutic applications of the antigene strategy in vivo.

In recent years, triplex DNA has attracted considerable interest because of its possible biological functions in vivo and its wide variety of potential applications, such as regulation of gene expression, site-specific cleavage of duplex DNA, mapping of genomic DNA, and gene-targeted mutagenesis (*1*−*3*). A triplex is usually formed through the sequence-specific interaction of a single-stranded homopurine or homopyrimidine triplex-forming oligonucleotide (TFO)[1] with the major groove of homopurine−homopyrimidine stretch in duplex DNA (*1*−*5*). In the pyrimidine motif triplex, a homopyrimidine TFO binds parallel to the homopurine strand of the target duplex by Hoogsteen hydrogen bonding to form T·A:T and C^+·G:C triplets (*1*−*5*). On the other hand, in the purine motif triplex, a homopurine TFO binds antiparallel to the homopurine strand of the target duplex by reverse Hoogsteen hydrogen bonding to form A·A:T (or T·A:T) and G·G:C triplets (*1*−*5*). The stability of triplex is affected by various environmental conditions, such as pH, temperature, ionic strength, and supercoil density (*1*−*9*).

Various kinds of chemical modifications in base, sugar moiety, and phosphate backbone have been developed to enhance the binding affinity of triplex formation under physiological condition (reviewed in refs *3* and *10*−*12*). To overcome the requirement of acidic pH for the pyrimidine motif triplex formation and to stabilize the pyrimidine motif triplex at neutral pH, several base analogues have been synthesized, such as 5-methylcytosine, N^6-methyl-8-oxo-2′-deoxyadenosine, and 2′-*O*-methylpseudoisocytidine. Modifications in sugar moiety have also been developed. RNA is the most obvious example of the substitution on the deoxyribose sugar moiety. To avoid degradation of RNA by nuclease, 2′-*O*-methyl-RNA has been designed in which the 2′ position of sugar moiety is replaced with a methoxy group. To change the electrostatic properties of negative phosphodiester backbone of natural DNA molecules and to achieve greater degrees of nuclease resistance and cell membrane permeability, several backbone modifications have been designed, such as phosphorothioate backbone and peptide nucleic acid.

As part of the search for nuclease-stable backbone modifications, N3′→P5′ phosphoramidate (PN) linkages (Figure 1a) have been developed (*13*−*21*). A TFO with PN linkages binds to target duplex DNA to form triplex DNA (*13, 14, 16*−*19, 21*). The thermal stability of the triplex with PN TFO was much higher than that with the corresponding natural phosphodiester (PO) TFO, which was shown by UV melting to analyze the denaturation process of the triplexes far above physiological temperature (*14, 16, 19*). However,

† This research was supported in part by Grant-in-Aid from the Ministry of Education, Science, Sports, and Culture of Japan (08249247 and 12217158).

* To whom correspondence should be addressed. Telephone: 81-298-36-9082. Fax: 81-298-36-9080. E-mail: torigoe@rtc.riken.go.jp.

[1] Abbreviations: TFO, triplex-forming oligonucleotide; PN, N3′→P5′ phosphoramidate; PO, natural phosphodiester; EMSA, electrophoretic mobility shift assay; ITC, isothermal titration calorimetry; IAsys, interaction analysis system; Pur23A·Pyr23T, 23-mer target duplex DNA; Pyr15T, 15-mer DNA as unmodified homopyrimidine TFO; Pyr15NP, 15-mer DNA with the same sequence as Pyr15T but with N3′→P5′ phosphoramidate backbone; Bt-Pyr23T, biotinylated Pyr23T.

10.1021/bi001895v CCC: $20.00
Published on Web 12/30/2000

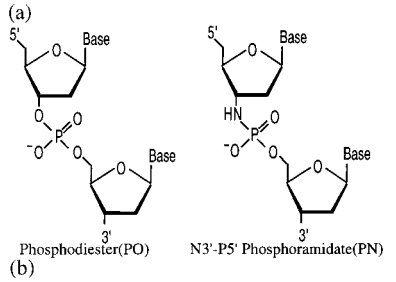

FIGURE 1: (a) Structural formula of phosphodiester (PO) and N3′→P5′ phosphoramidate (PN) backbones. (b) Oligonucleotide sequences of the target duplex (Pur23A·Pyr23T), the specific TFOs (Pyr15T and Pyr15NP), and the nonspecific oligonucleotide (Pyr15NS).

the formation process of the triplex involving PN TFO near physiological temperature has not been well-characterized yet. To apply triplex as an antigene drug for artificial control of gene expression in vivo, the investigation of the formation process of triplex near physiological temperature may be more important than that of the denaturation process of triplex far above physiological temperature. In addition, the mechanistic explanation for the PN modification-mediated triplex stabilization has not been clearly understood.

I have previously analyzed the thermodynamic and kinetic effects of four chemical modifications of TFO on pyrimidine motif triplex formation with the same target duplex at room temperature, demonstrating that the modification of phosphate backbone of TFO produced a more significant effect on the thermodynamics and kinetics of the triplex formation than the modifications of base and sugar moiety (*22*). In the present study, I have further extended the previous study to explore the thermodynamic and kinetic effects of another backbone modification, PN modification, of TFO on pyrimidine motif triplex formation at room temperature. The thermodynamic and kinetic properties of the pyrimidine motif triplex formation between a 23-bp homopurine−homopyrimidine target duplex (Pur23A·Pyr23T) (Figure 1b) and its specific 15-mer homopyrimidine PO TFO (Pyr15T) or PN TFO (Pyr15NP) (Figure 1b) have been examined by electrophoretic mobility shift assay (EMSA) (*23*, *24*), UV melting, isothermal titration calorimetry (ITC) (*9*, *22*, *24*−*28*), and interaction analysis system (IAsys) (*22*, *24*, *28*−*31*). I have found that the PN modification of TFO increased the binding constant of the pyrimidine motif triplex formation at room temperature and neutral pH by nearly 2 orders of magnitude. Kinetic analyses have demonstrated that the major contribution for the increase in the binding constant of the triplex formation resulted from the considerable decrease in the dissociation rate constant rather than the increase in the association rate constant. The ability of the PN modification to promote pyrimidine motif triplex formation near physiological temperature and pH would support further progress in therapeutic applications of the antigene strategy in vivo. The mechanism of the PN modification to promote pyrimidine motif triplex formation will be discussed.

MATERIALS AND METHODS

Preparation of Oligonucleotides. I synthesized 23-mer complementary oligonucleotides for target duplex, Pur23A and Pyr23T (Figure 1b); a 15-mer homopyrimidine PO TFO specific for the target duplex, Pyr15T (Figure 1b); and a nonspecific oligonucleotide, Pyr15NS (Figure 1b), on an ABI DNA synthesizer using the solid-phase cyanoethyl phosphoramidite method and purified them with reverse-phase high-performance chromatography on a Wakosil DNA column. A 15-mer homopyrimidine PN TFO specific for the target duplex, Pyr15NP (Figure 1b), was synthesized and purified as described previously (*13*, *15*, *20*). 5′-Biotinylated Pyr23T (denoted as Bt-Pyr23T) was prepared using biotin phosphoramidite. The concentration of all oligonucleotides was determined by UV absorbance. Complementary strands, Pur23A and Pyr23T, were annealed by heating at up to 90 °C, followed by a gradual cooling to room temperature. The annealed sample was applied on a hydroxyapatite column (KOKEN Inc.) to remove unpaired single strands. The concentration of the duplex DNA (Pur23A·Pyr23T) was determined by UV absorption considering the DNA concentration ratio of 1 OD = 50 μg/mL, with a M_r of 15 180.

Electrophoretic Mobility Shift Assay (*EMSA*). EMSA experiments were performed essentially as described previously (*24*). In 9 μL of reaction mixture, a ^{32}P-labeled Pur23A·Pyr23T duplex (∼10 pg) was mixed with increasing concentrations of the specific TFO (Pyr15T or Pyr15NP) and the nonspecific oligonucleotide (Pyr15NS) in buffer [50 mM Tris−acetate (pH 7.0), 100 mM NaCl, and 10 mM $MgCl_2$]. Pyr15NS was added to achieve equimolar concentrations of TFO in each lane as well as to minimize adhesion of the DNA (duplex and TFO) to plastic surfaces during incubation and subsequent losses during processing. After 6 h incubation at 37 °C, 2 μL of 50% glycerol solution containing bromophenol blue was added without changing the pH and salt concentrations of the reaction mixtures. Samples were then directly loaded onto a 15% native polyacrylamide gel prepared in buffer [50 mM Tris−acetate (pH 7.0) and 10 mM $MgCl_2$], and electrophoresis was performed at 8 V/cm for 16 h at 4 °C.

UV Melting. UV melting experiments were carried out on a JASCO Ubest-30 spectrophotometer equipped with a EHC-363 Peltier type cell holder controlled by a TPU-436 temperature programmer. UV melting profiles were measured in buffer A (10 mM sodium cacodylate−cacodylic acid at pH 6.8 containing 200 mM NaCl and 20 mM $MgCl_2$) at a scan rate of 0.5 °C/min at 260 nm. The first derivative was calculated from the UV melting profile. The peak temperatures in the derivative curve were designated as the melting temperature, T_m. Cell path length was 1 cm. The triplex DNA concentration used was 1 μM.

CD Spectroscopy and CD Melting. CD spectra were recorded in buffer A on a JASCO J-720 spectropolarimeter interfaced with a microcomputer. CD melting experiments were performed in the same buffer at a scan rate of 1 °C/min at 220 nm on the same spectropolarimeter by controlling the sample temperature with a Peltier type temperature controller. The first derivative was calculated from the CD melting profile. The peak temperatures in the derivative curve were designated as the melting temperature, T_m. Cell path length was 5 mm. The triplex DNA concentration used was 2 μM.

Isothermal Titration Calorimetry (*ITC*). Isothermal titration experiments were carried out on a MCS ITC system (Microcal Inc., U.S.A.), essentially as described previously (*9*, *22*, *24*). The TFO and Pur23A·Pyr23T duplex solutions were prepared by extensive dialysis against buffer A or buffer B (10 mM sodium cacodylate−cacodylic acid at pH 5.8 containing 200 mM NaCl and 20 mM $MgCl_2$). The TFO solution in buffer A or buffer B was injected in 5-μL increments and 10-min intervals into the Pur23A·Pyr23T duplex solution without changing the reaction conditions. The heat for each injection was subtracted by the heat of dilution of the injectant, which was measured by injecting the TFO solution into the same buffer. Each corrected heat was divided by the moles of the TFO solution injected and analyzed with Microcal Origin software supplied by the manufacturer.

Interaction Analysis System (*IAsys*). Kinetic experiments by resonant mirror method were performed on an IAsys Plus instrument (Affinity Sensors Cambridge Inc., U.K.), essentially as described previously, where a real-time biomolecular interaction was measured with a laser biosensor (*22*, *24*). The resonant layer of a cuvette was washed with 80 μL of 10 mM acetate buffer (pH 4.6) and then activated with 80 μL of a mixture of 1-ethyl-3-(3-dimethylaminopropyl) carbodiimide and *N*-hydroxysuccinimide solution. The activated surface was again washed with 10 mM acetate buffer (pH 4.6), and streptavidin in 10 mM acetate buffer (pH 4.6) was immobilized to the surface. After the remaining reactive groups were blocked with 1 M ethanolamine (pH 8.5), the cuvette was extensively washed with 10 mM acetate buffer (pH 4.6) and then with 20 mM HCl to remove the loosely associated protein. The cuvette was washed with buffer A, and Bt-Pyr23T (1.2 μM in buffer A) was added to bind with the streptavidin on the surface. After washing the cuvette with the same buffer, the complementary oligonucleotide, Pur23A (1.2 μM in buffer A), was added to hybridize with Bt-Pyr23T. After extensive washing and equilibrating the Bt-Pyr23T·Pur23A-immobilized surface with buffer A for more than 30 min, the TFO in 80 μL of buffer A was injected over the immobilized Bt-Pyr23T·Pur23A duplex, and then the triplex formation was monitored for 30 min. This was followed by washing the cuvette with buffer A, and the dissociation of the preformed triplex was monitored for an additional 20 min. Finally, 10 mM NaOH was injected for 3 min for a complete break of the Hoogsteen hydrogen bonding between the TFO and Pur23A, during which the Bt-Pyr23T·Pur23A duplex may be partially denatured. The Bt-Pyr23T·Pur23A duplex was regenerated by injecting 1.2 μM Pur23A. The resulting sensorgrams were analyzed with the Fastfit software supplied by the manufacturer to calculate the kinetic parameters.

RESULTS

Electrophoretic Mobility Shift Assay of Pyrimidine Motif Triplex Formation. The pyrimidine motif triplex formation of the target duplex (Pur23A·Pyr23T; Figure 1b) with the specific TFO (Pyr15T or Pyr15NP; Figure 1b) was examined at pH 7.0 by EMSA (Figure 2). The total oligonucleotide concentration ([specific TFO (Pyr15T or Pyr15NP; Figure 1b)] + [nonspecific oligonucleotide (Pyr15NS; Figure 1b)]) was kept constant at 10 μM to minimize losses of DNA during processing. While incubation with 10 μM Pyr15NS alone did not cause a shift in electrophoretic migration of the target duplex (see lane 1 for each condition), those with Pyr15T or Pyr15NP at particular concentration caused retardation of the duplex migration because of triplex formation (*23*). The dissociation constant, K_d, of triplex formation was determined from the concentration of the TFO, which caused half of the target duplex to shift to the triplex (*23*). The K_d of the triplex with Pyr15T was estimated to be about 10^{-6} M. In contrast, the K_d of the triplex with Pyr15NP was about 10^{-8} M, indicating that the PN modification of TFO increased the binding affinity of the pyrimidine motif triplex formation at neutral pH by nearly 2 orders of magnitude.

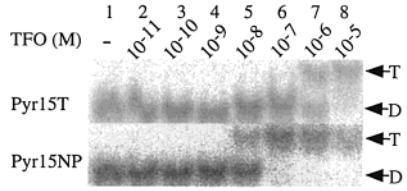

FIGURE 2: EMSA of the pyrimidine motif triplex formation with the specific TFO (Pyr15T or Pyr15NP) at neutral pH. Triplex formation was initiated by adding ^{32}P-labeled Pur23A·Pyr23T duplex (~10 pg) with the indicated final concentrations of the specific TFO (Pyr15T or Pyr15NP). The nonspecific oligonucleotide (Pyr15NS) was added to adjust the equimolar concentrations of TFO (Pyr15T + Pyr15NS or Pyr15NP + Pyr15NS) (10 μM) in each lane. The reaction mixtures with Pyr15T or Pyr15NP in the buffer [50 mM Tris−acetate (pH 7.0), 100 mM NaCl, and 10 mM $MgCl_2$] were incubated for 6 h at 37 °C and then electrophoretically separated on a 15% native polyacrylamide gel at 4 °C. The positions of the duplex (D) and triplex (T) are indicated.

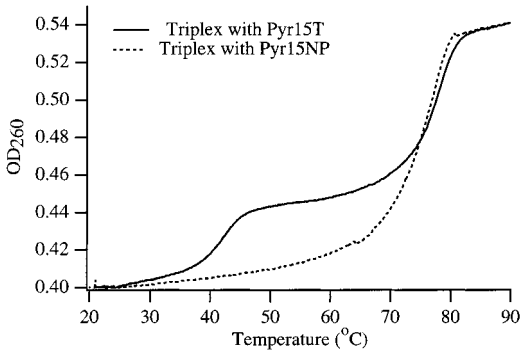

FIGURE 3: UV melting profiles of the pyrimidine motif triplex with the specific TFO (Pyr15T or Pyr15NP) at neutral pH. The triplexes with Pyr15T or Pyr15NP in buffer A were melted at a scan rate of 0.5 °C/min with detection at 260 nm. Cell path length was 1 cm. The triplex DNA concentration used was 1 μM.

Spectroscopic Characterization of Pyrimidine Motif Triplex. The thermal stability of the pyrimidine motif triplex with Pyr15T or Pyr15NP was investigated at pH 6.8 by UV melting (Figure 3). The triplex with Pyr15T showed two-step melting. The first transition at lower temperature, T_{m1} (42 °C), was the melting of the triplex to a duplex and a TFO, and the second transition at higher temperature, T_{m2} (77 °C), was the melting of the duplex. On the other hand, the triplex with Pyr15NP showed only one transition at higher temperature, T_m = 77 °C. As the magnitude in UV absorbance change at T_m for Pyr15NP was almost equal to the sum of those at T_{m1} and T_{m2} for Pyr15T (Figure 3), the transition was identified as a direct melting of the triplex to its constituting single-strand DNAs. The PN modification

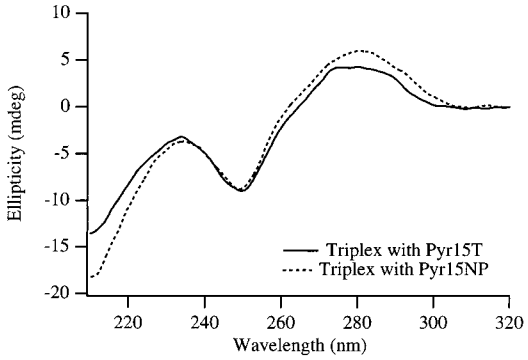

FIGURE 4: CD spectra of the pyrimidine motif triplex with the specific TFO (Pyr15T or Pyr15NP) at neutral pH. The triplexes with Pyr15T or Pyr15NP at 15 °C and pH 6.8 in buffer A were measured in the wavelength range of 210−320 nm. Cell path length was 5 mm. The triplex DNA concentration used was 2 μM.

therefore increased the melting temperature of the triplex by 35 °C, confirming, like others (*14*, *16*, *19*), that the PN modification of TFO increased the thermal stability of the pyrimidine motif triplex at neutral pH.

To further characterize the triplexes involving Pyr15T or Pyr15NP, CD spectra (Figure 4) and CD melting (data not shown) of the triplexes were measured. A negative band in the short-wavelength (210−220 nm) region was observed for both CD profiles at 15 °C and pH 6.8 (Figure 4), confirming the triplex formation involving Pyr15T or Pyr15NP (*32*). The overall shape of the CD spectra was quite similar between the two profiles (Figure 4), suggesting that no significant change may be induced in the higher order structure of the pyrimidine motif triplex by the PN modification. The melting temperature of the triplexes at pH 6.8 measured by CD melting (data not shown) was consistent with those obtained from the UV melting described above.

Thermodynamic Analyses of Pyrimidine Motif Triplex Formation by ITC. I examined the thermodynamic parameters of the pyrimidine motif triplex formation between a 23-bp target duplex (Pur23A·Pyr23T) and its specific 15-mer TFO (Pyr15T or Pyr15NP) at 25 °C and pH 6.8 by ITC. To investigate the pH dependence of the pyrimidine motif triplex formation, the thermodynamic parameters of the triplex formation between Pur23A·Pyr23T and Pyr15T were also analyzed at 25 °C and pH 5.8 by ITC. Figure 5a shows a typical ITC profile for the interaction between Pyr15NP and Pur23A·Pyr23T at 25 °C and pH 6.8. An exothermic heat pulse was observed after each injection of Pyr15NP into Pur23A·Pyr23T. The magnitude of each peak decreased gradually with each new injection, and an endothermic peak was still observed at a molar ratio of [Pyr15NP]/[Pur23A·Pyr23T] = 2. The endothermic peak was proved to be the heat of dilution of Pyr15NP by a blank experiment in the absence of Pur23A·Pyr23T. The area under each peak was integrated, and the heat of dilution of Pyr15NP was subtracted from the integrated values. The corrected heat was divided by the moles of each injection, and the resulting values were plotted as a function of molar ratio of [Pyr15NP]/[Pur23A·Pyr23T], as shown in Figure 5b. The resultant titration plot was fitted to a sigmoidal curve by a nonlinear least-squares method. The binding constant, K_a, and the enthalpy change, ΔH, were obtained from the fitted curve (*27*). The Gibbs free energy change, ΔG, and the entropy change, ΔS, were calculated from the equation $\Delta G = -RT$

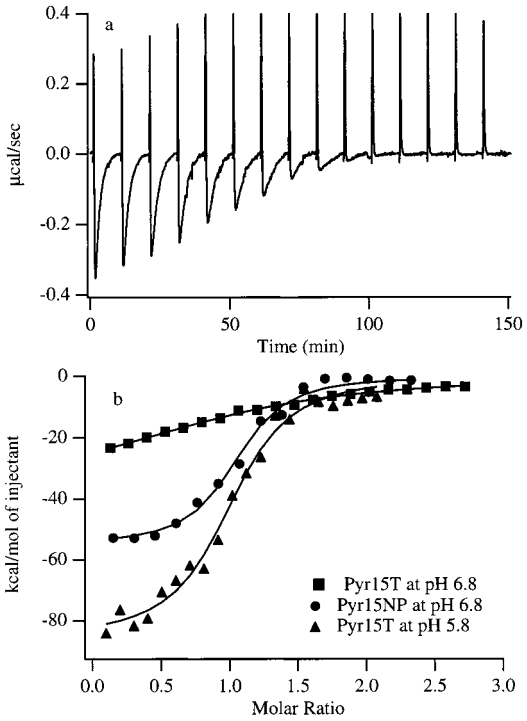

FIGURE 5: Thermodynamic analyses of the pyrimidine motif triplex formation with Pyr15T or Pyr15NP at pH 6.8 and with Pyr15T at pH 5.8 by ITC. (a) Typical profiles for the triplex formation between Pyr15NP and Pur23A·Pyr23T at 25 °C and pH 6.8. The Pyr15NP solution (195 μM in buffer A) was injected 15 times in 5-μL increments into 5 μM Pur23A·Pyr23T solution, which was dialyzed against the same buffer. Injections were occurred over 10 s at 10-min intervals. (b) The titration plots against the molar ratio of [TFO]/[Pur23A·Pyr23T]. The data were fitted by a nonlinear least-squares method.

ln $K_a = \Delta H - T\Delta S$ (*27*). The titration plots for Pyr15T at pH 5.8 and pH 6.8 are also shown in Figure 5b. The thermodynamic parameters for Pyr15T at pH 5.8 and pH 6.8 were obtained from the titration plots in the same way.

Table 1 summarizes the thermodynamic parameters for the pyrimidine motif triplex formation with Pyr15T or Pyr15NP at 25 °C and pH 6.8 and those with Pyr15T at 25 °C and pH 5.8, obtained from ITC. The signs of both ΔH and ΔS were negative under all the conditions. Because an observed negative ΔS was unfavorable for the triplex formation, the triplex formation was driven by a large negative ΔH under each condition. The magnitudes of the negative ΔH of the triplex formation for Pyr15T at pH 5.8 and for Pyr15NP at pH 6.8 were 2.5 or 1.7 times larger than that observed for Pyr15T at pH 6.8. The K_a for Pyr15T at pH 5.8 was about 20 times larger than that observed for Pyr15T at pH 6.8, confirming, like others (*7*, *33*, *34*), that neutral pH is unfavorable for the pyrimidine motif triplex formation involving C^+·G:C triads. In addition, the K_a for Pyr15NP at pH 6.8 was about 30 times larger than that observed for Pyr15T at pH 6.8, indicating that the PN modification of TFO increased the K_a of the pyrimidine motif triplex formation at neutral pH, which was consistent with the result of EMSA (Figure 2).

Kinetic Analyses of Pyrimidine Motif Triplex Formation by IAsys. To examine the putative mechanism involved in the increase in K_a of the pyrimidine motif triplex formation by the PN modification (Figure 2 and Table 1), I assessed the kinetic parameters for the association and dissociation

Table 1: Thermodynamic Parameters for the Pyrimidine Motif Triplex Formation with Pyr15T or Pyr15NP at 25 °C, Obtained from ITC

TFO	pH	K_a (M^{-1})	K_a (relative)	ΔG (kcal mol^{-1})	ΔH (kcal mol^{-1})	ΔS (cal mol^{-1} K^{-1})
Pyr15T	5.8[a]	$(3.83 \pm 0.74) \times 10^6$	19.4	-8.98 ± 0.13	-85.6 ± 2.6	-257 ± 9.1
Pyr15T	6.8[b]	$(1.97 \pm 0.43) \times 10^5$	1.0	-7.22 ± 0.15	-34.9 ± 2.2	-92.7 ± 8.0
Pyr15NP	6.8[b]	$(5.58 \pm 1.12) \times 10^6$	28.3	-9.20 ± 0.13	-59.7 ± 2.0	-169 ± 7.0

[a] 10 mM sodium cacodylate-cacodylic acid (pH 5.8), 200 mM sodium chloride, and 20 mM magnesium chloride. [b] 10 mM sodium cacodylate-cacodylic acid (pH 6.8), 200 mM sodium chloride, and 20 mM magnesium chloride.

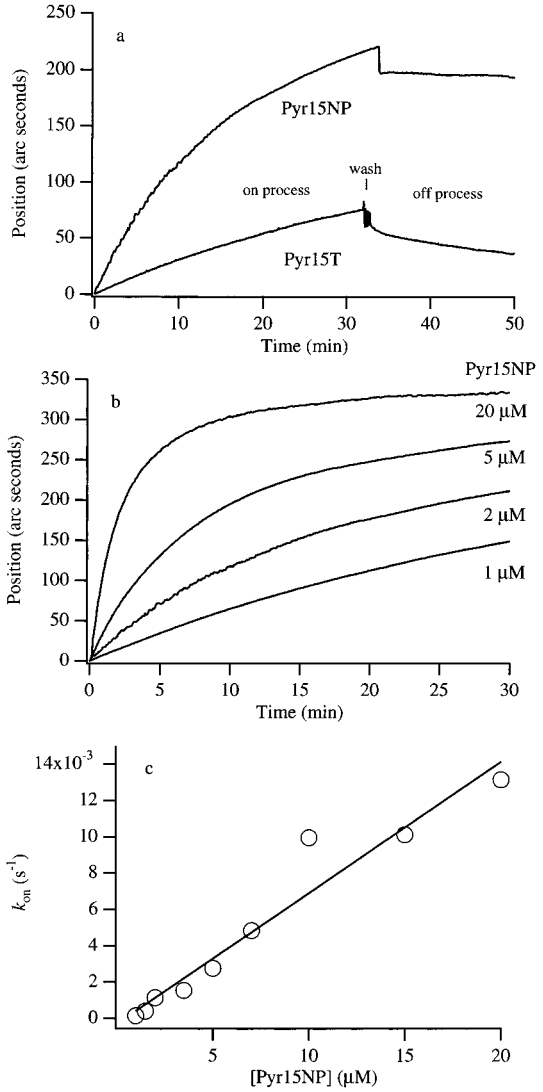

FIGURE 6: Kinetic analyses of the pyrimidine motif triplex formation with the specific TFO (Pyr15T or Pyr15NP) at neutral pH by IAsys. (a) Typical sensorgrams for the triplex formation at 25 °C and pH 6.8 after injecting 2.0 μM specific TFO (Pyr15T or Pyr15NP) into the Bt-Pyr23T·Pur23A-immobilized cuvette are shown. (b) A series of sensorgrams for the triplex formation between Pyr15NP and Pur23A·Pyr23T at 25 °C and pH 6.8. The Pyr15NP solution, diluted in buffer A to achieve the indicated final concentrations, were injected into the Bt-Pyr23T·Pur23A-immobilized cuvette. The binding of Pyr15NP to Bt-Pyr23T·Pur23A was monitored as the response against time. (c) Measured on-rate constants, k_{on}, of the triplex formation in panel b were plotted against the respective concentrations of Pyr15NP. The plot was fitted to a straight line ($r^2 = 0.97$) by a linear least-squares method.

of TFO (Pyr15T or Pyr15NP) with Pur23A·Pyr23T at 25 °C and pH 6.8 by IAsys. Figure 6a compares the sensorgrams representing the triplex formation and dissociation involving 2.0 μM of the specific TFO (Pyr15T or Pyr15NP). The injection of Pyr15T over the immobilized Bt-Pyr23T·Pur23A duplex caused an increase in response. Although the change in the association curve for Pyr15NP was moderately enhanced, the change in the dissociation curve with time for Pyr15NP was very much smaller than that for Pyr15T. The result indicated that the PN modification of TFO remarkably decreased the dissociation rate constant of the triplex equilibrium.

To understand the kinetic parameters more quantitatively, I analyzed a series of association and dissociation curves at the various concentrations of TFO. As shown in Figure 6b, an increase in the concentration of Pyr15NP led to a gradual change in the response of the association curves. The on-rate constant (k_{on}) was obtained from the analysis of each association curve. Figure 6c shows a plot of k_{on} against the Pyr15NP concentrations. The association rate constant (k_{assoc}) was determined from the slope of the fitted line obtained by a linear least-squares method (*29*−*31*). The off-rate constant (k_{off}) was obtained from the analysis of each dissociation curve (Figure 6a and data not shown). Because k_{off} is usually independent of the concentration of the injected solution, the dissociation rate constant (k_{dissoc}) was determined by averaging k_{off} for several concentrations (*29*−*31*). K_a was calculated from the equation, $K_a = k_{assoc}/k_{dissoc}$. The kinetic parameter for Pyr15T was obtained in the same way.

Table 2 summarizes the kinetic parameters for the pyrimidine motif triplex formation with Pyr15T or Pyr15NP at 25 °C and pH 6.8, obtained from IAsys. The magnitudes of K_a calculated from the ratio of k_{assoc} to k_{dissoc} (Table 2) were consistent with those obtained from ITC (Table 1). The K_a for Pyr15NP at pH 6.8 was about 70 times larger than that observed for Pyr15T at pH 6.8, indicating that the PN modification of TFO increased the K_a of the pyrimidine motif triplex formation at neutral pH, which supported the results of EMSA (Figure 2) and ITC (Table 1). The PN modification of TFO decreased k_{dissoc} by about 35 times, while it moderately increased k_{assoc} by no more than 2 times. Thus, the much larger K_a by the PN modification of TFO resulted mainly from the decrease in k_{dissoc} rather than the increase in k_{assoc}.

DISCUSSION

The K_a of the pyrimidine motif triplex formation with Pyr15T at pH 5.8 was 20 times larger than that observed with Pyr15T at pH 6.8 (Table 1), which is consistent with the previously reported results that neutral pH is unfavorable for the pyrimidine motif triplex formation involving C^+·GC triads (*7*, *33*, *34*). The K_a of the triplex formation with Pyr15NP at pH 6.8 was 30 times larger than that observed with Pyr15T at pH 6.8 (Table 1). The increase in K_a at pH 6.8 by the PN modification of TFO was supported by the results of EMSA (Figure 2) and IAsys (Table 2). In addition, the PN modification of TFO increased the thermal stability of the pyrimidine motif triplex at pH 6.8 (Figure 3), which

Table 2: Kinetic Parameters for the Pyrimidine Motif Triplex Formation with Pyr15T or Pyr15NP at 25 °C and pH 6.8 in 10 mM Sodium Cacodylate−Cacodylic Acid, 200 mM Sodium Chloride, and 20 mM Magnesium Chloride, Obtained from IAsys

TFO	k_{assoc} (M^{-1} s^{-1})	k_{assoc} (relative)	k_{dissoc} (s^{-1})	k_{dissoc} (relative)	K_a (M^{-1})	K_a (relative)
Pyr15T	$(6.31 \pm 0.18) \times 10^2$	1.0	$(1.17 \pm 0.14) \times 10^{-2}$	1.0	$(5.41 \pm 0.91) \times 10^4$	1.0
Pyr15NP	$(1.19 \pm 0.13) \times 10^3$	1.89	$(3.36 \pm 0.18) \times 10^{-4}$	0.029	$(3.54 \pm 0.61) \times 10^6$	65.4

confirms the results obtained by other groups (*14*, *16*, *19*). These results indicate that the PN modification of TFO considerably promotes the pyrimidine motif triplex formation at neutral pH.

The ΔH upon the triplex formation measured by ITC reflects a major contribution from the hydrogen bonding and the base stacking involved in the triplex formation (*9*, *35*−*37*). On the other hand, the ΔS upon the triplex formation measured by ITC includes a positive entropy change from release of structured water upon the triplex formation and a major contribution of a negative conformational entropy change from the conformational restraint of TFO upon the triplex formation (*9*, *35*−*37*). The magnitudes of ΔH and ΔS upon the triplex formation with Pyr15T at pH 6.8 were considerably smaller than those observed with Pyr15T at pH 5.8 or with Pyr15NP at pH 6.8 (Table 1), indicating that the pyrimidine motif triplex formation with Pyr15T at pH 6.8 was significantly less stoichiometric than that with Pyr15T at pH 5.8 or with Pyr15NP at pH 6.8. In contrast, as can be judged from the magnitudes of the thermodynamic parameters (Table 1), the pyrimidine motif triplex formed almost stoichiometrically with Pyr15NP at pH 6.8 as well as with Pyr15T at pH 5.8.

The K_a and ΔG for the stoichiometric triplex formations with Pyr15NP at pH 6.8 and with Pyr15T at pH 5.8 were quite similar (Table 1). However, the ingredients of ΔG, that is, ΔH and ΔS, were obviously different from each other. The magnitudes of the negative ΔH and ΔS for Pyr15NP at pH 6.8 were smaller than those observed for Pyr15T at pH 5.8 (Table 1). The hydrogen bonding and the base stacking involved in the triplex formation, and the immobilization of electrostricted water molecules around polar atoms upon the triplex formation are usually considered to be the major sources of the negative ΔH upon the triplex formation (*9*, *35*−*37*). Thus, the difference in ΔH for the stoichiometric triplex formations between Pyr15NP at pH 6.8 and Pyr15T at pH 5.8 (Table 1) suggests that the hydrogen bonding and/or the base stacking of the triplex with the PN TFO and the degree of the immobilization of water molecules around the protonated cytosines and polar nitrogen atoms of the triplex with the PN TFO may be significantly different from those with the corresponding PO TFO. On the other hand, the negative ΔS upon the triplex formation is mainly contributed by a negative conformational entropy change due to the conformational restraint of TFO involved in the triplex formation (*9*, *35*−*37*). Therefore, the fact concerning the stoichiometric triplex formations that the magnitude of the negative ΔS for Pyr15NP at pH 6.8 was smaller than that for Pyr15T at pH 5.8 (Table 1) suggests that the PN TFO in the free state may be more rigid than the corresponding PO TFO.

The temperature dependence of the K_a value of the triplex formation involving Pyr15NP at pH 6.8 was examined in the range of 15−30 °C by ITC (data not shown). On the basis of the data, the van't Hoff enthalpy change, ΔH_{VH}, for the triplex formation involving Pyr15NP at pH 6.8 was positive (15.9 kcal mol^{-1}) by the equation $\Delta H_{VH} = -R\,\delta \ln K_a/\delta(1/T)$. The positive ΔH_{VH} was in sharp contrast with the large negative calorimetric enthalpy change, ΔH_{cal}, shown in Table 1. The significant discrepancy between ΔH_{VH} and ΔH_{cal} suggests a possibility that the triplex formation involving Pyr15NP at pH 6.8 may not be a simple two-state binding process and that an intermediate state may be involved in the triplex formation (*9*). The more rigidity of the PN TFO in the free state might be related to the intermediate state upon the triplex formation.

Because the K_a of the pyrimidine motif triplex formation at pH 6.8 was increased by the PN modification (Figure 2 and Tables 1 and 2), the PN modification has the ability to stabilize the pyrimidine motif triplex at neutral pH. The more rigidity of the PN TFO in the free state relative to the corresponding PO TFO discussed above causes the smaller entropic loss upon the triplex formation with the PN TFO at neutral pH, which provides a favorable component to the K_a and ΔG, and leads to the increase in the K_a. The favorable smaller entropic loss upon the triplex formation due to the more rigidity of the PN TFO in the free state seems apparently contradictory to the ITC results (Table 1) that the apparent negative ΔS for the triplex formation with Pyr15NP at pH 6.8 was decreased in comparison with that observed with Pyr15T at pH 6.8. However, the apparent contradiction seems feasible, because the stoichiometric triplex formation with Pyr15NP at pH 6.8 would result in the larger magnitude of negative conformational entropy change due to the more amount of conformationally restrained TFO upon the triplex formation than the significantly less stoichiometric triplex formation with Pyr15T at pH 6.8. We conclude that the more rigidity of the PN TFO in the free state may be a factor to increase the K_a of the pyrimidine motif triplex formation at neutral pH.

Kinetic data have demonstrated that the PN modification of TFO considerably decreased the k_{dissoc} of the pyrimidine motif triplex formation at neutral pH (Table 2). The decrease in the k_{dissoc} is a plausible kinetic reason to explain the remarkable gain in the K_a at neutral pH by the PN modification (Figure 2 and Tables 1 and 2). Both our group (*9*) and others (*38*) have previously proposed a model that triplexes form along nucleation−elongation processes: in a nucleation step only a few base contacts of the Hoogsteen hydrogen bonds may be formed between TFO and the target duplex, and this may be followed by an elongation step in which Hoogsteen base pairings progress to complete triplex formation. Both groups (*9*, *38*) have also suggested that the observed K_a, which is the ratio of k_{assoc} to k_{dissoc}, may mostly reflect a rapid equilibrium of the nucleation step, which is probably the rate-limiting process of the triplex formation. In this sense, the PN modification is considered to slow the collapse of the nucleation intermediate using the rigidity of PN TFO to increase the K_a of the pyrimidine motif triplex formation.

I previously examined the thermodynamic and kinetic effects of four chemical modifications of TFO on pyrimidine motif triplex formation at room temperature with the same target duplex (Pur23A·Pyr23T) (*22*). I suggested that the modification of phosphate backbone of TFO produced a more significant effect on the thermodynamics and kinetics of the triplex formation than the modifications of base and sugar moiety (*22*). In the present study, I have further extended the previous study to explore the thermodynamic and kinetic effects of another backbone modification, PN modification, of TFO on pyrimidine motif triplex formation at room temperature. The PN modification of TFO increased the K_a of the pyrimidine motif triplex formation near physiological temperature and pH by nearly 2 orders of magnitude, which mainly resulted from the considerable decrease in the k_{dissoc}. The more rigidity of the PN TFO in the free state may enable the significant increase in the K_a of the pyrimidine motif triplex formation under physiological condition. This information will present an effective approach for designing chemically modified TFO with higher binding affinity in the triplex formation under physiological conditions, which may eventually lead to progress in therapeutic applications of the antigene strategy in vivo.

ACKNOWLEDGMENT

I gratefully acknowledge Dr. Atsushi Maruyama for generous help with the use of CD spectropolarimeter and for critical reading of the manuscript and helpful discussion. I thank Dr. Koko Mizumachi for generous consideration concerning the use of IAsys Plus instrument. I am also grateful to Mr. Ryuji Shimizume for helpful technical assistance.

REFERENCES

1. Mirkin, S. M., and Frank-Kamenetskii, M. D. (1994) *Annu. Rev. Biophys. Biomol. Struct. 23*, 541−576.
2. Frank-Kamenetskii, M. D., and Mirkin, S. M. (1995) *Annu. Rev. Biochem. 64*, 65−95.
3. Soyfer, V. N., and Potaman, V. N. (1996) *Triple-Helical Nucleic Acids*, Springer-Verlag, New York.
4. Sun, J.-S., and Helene, C. (1993) *Curr. Opin. Struct. Biol. 3*, 345−356.
5. Sun, J.-S., Garestier, T., and Helene, C. (1996) *Curr. Opin. Struct. Biol. 6*, 327−333.
6. Plum, G. E., Pilch, D. S., Singleton, S. F., and Breslauer, K. J. (1995) *Annu. Rev. Biophys. Biomol. Struct. 24*, 319−350.
7. Shindo, H., Torigoe, H., and Sarai, A. (1993) *Biochemistry 32*, 8963−8969.
8. Sarai, A., Sugiura, S., Torigoe, H., and Shindo, H. (1993) *J. Biomol. Struct. Dyn. 11*, 245−252.
9. Kamiya, M., Torigoe, H., Shindo, H., and Sarai, A. (1996) *J. Am. Chem. Soc. 118*, 4532−4538.
10. Mesmaeker, A. D., Altmann, K.-H., Waldner, A., and Wendeborn, S. (1995) *Curr. Opin. Struct. Biol. 5*, 343−355.
11. Nielsen, P. E. (1995) *Annu. Rev. Biophys. Biomol. Struct. 24*, 167−183.
12. Fox, K. R. (2000) *Curr. Med. Chem. 7*, 17−37.
13. Gryaznov, S., and Chen, J.-K. (1994) *J. Am. Chem. Soc. 116*, 3143−3144.
14. Gryaznov, S. M., Lloyd, D. H., Chen, J.-K., Schultz, R. G., DeDionisio, L. A., Ratmeyer, L., and Wilson, W. D. (1995) *Proc. Natl. Acad. Sci. U.S.A. 92*, 5798−5802.
15. Chen, J.-K., Schultz, R. G., Lloyd, D. H., and Gryaznov, S. M. (1995) *Nucleic Acids Res. 23*, 2661−2668.
16. Escude, C., Giovannangeli, C., Sun, J.-S., Lloyd, D. H., Chen, J.-K., Gryaznov, S. M., Garestier, T., and Helene, C. (1996) *Proc. Natl. Acad. Sci. U.S.A. 93*, 4365−4369.
17. Giovannangeli, C., Perrouault, L., Escude, C., Gryaznov, S., and Helene, C. (1996) *J. Mol. Biol. 261*, 386-398.
18. Giovannangeli, C., Diviacco, S., Labrousse, V., Gryaznov, S., Charneau, P., and Helene, C. (1997) *Proc. Natl. Acad. Sci. U.S.A. 94*, 79−84.
19. Zhou-Sun, B., Sun, J.-S., Gryaznov, S. M., Liquier, J., Garestier, T., Helene, C., and Taillandier, E. (1997) *Nucleic Acids Res. 25*, 1782−1787.
20. Nelson, J. S., Fearon, K. L., Nguyen, M. Q., McCurdy, S. N., Frediani, J. E., Foy, M. F., and Hirschbein, B. L. (1997) *J. Org. Chem. 62*, 7278−7287.
21. Faria, M., Wood, C. D., Perrouault, L., Nelson, J. S., Winter, A., White, M. R. H., Helene, C., and Giovannangeli, C. (2000) *Proc. Natl. Acad. Sci. U.S.A. 97*, 3862−3867.
22. Torigoe, H., Shimizume, R., Sarai, A., and Shindo, H. (1999) *Biochemistry 38*, 14653−14659.
23. Lyamichev, V. I., Mirkin, S. M., Frank-Kamenetskii, M. D., and Cantor, C. R. (1988) *Nucleic Acids Res. 16*, 2165−2178.
24. Torigoe, H, Ferdous, A., Watanabe, H., Akaike, T., and Maruyama, A. (1999) *J. Biol. Chem. 274*, 6161−6167.
25. Langerman, N., and Biltonen, R. L. (1979) *Methods Enzymol. 61*, 261−286.
26. Biltonen, R. L., and Langerman, N. (1979) *Methods Enzymol. 61*, 287−318.
27. Wiseman, T., Williston, S., Brandts, J. F., and Lin, L.-N. (1989) *Anal. Biochem. 179*, 131−137.
28. Torigoe, H., Ferdous, A., Watanabe, H., Akaike, T., and Maruyama, A. (1999) *Nucleosides Nucleotides 18*, 1655−1656.
29. Cush, R., Cronin, J. M., Stewart, W. J., Maule, C. H., Molloy, J., and Goddard, N. J. (1993) *Biosens. Bioelectron. 8*, 347−353.
30. Edwards, P. R., Gill, A., Pollard-Knight, D. V., Hoare, M., Buckle, P. E., Lowe, P. A., and Leatherbarrow, R. J. (1995) *Anal. Biochem. 231*, 210−217.
31. Bates, P. J., Dosanjh, H. S., Kumar, S., Jenkins, T. C., Laughton, C. A., and Neidle, S. (1995) *Nucleic Acids Res. 23*, 3627−3632.
32. Manzini, G., Xodo, L. E., Gasparotto, D., Quadrifoglio, F., van der Marel, G. A., and van Boom, J. H. (1990) *J. Mol. Biol. 213*, 833−843.
33. Frank-Kamenetskii, M. D. (1992) *Methods Enzymol. 211*, 180−191.
34. Singleton, S. F., and Dervan, P. B. (1992) *Biochemistry 31*, 10995−11003.
35. Edelhoch, H., and Osborne, J. C., Jr. (1976) *Adv. Protein Chem. 30*, 183−250
36. Cheng, Y.-K., and Pettitt, B. M. (1992) *Prog. Biophys. Mol. Biol. 58*, 225−257.
37. Shafer, R. H. (1998) *Prog. Nucleic Acid Res. Mol. Biol. 59*, 55−94.
38. Rougee, M., Faucon, B., Mergny, J. L., Barcelo, F., Giovannangeli, C., Garestier, T., and Helene, C. (1992) *Biochemistry 31*, 9269−9278.

BI001895V